Type I and III interferons synergize with TNF to promote virally-triggered damage to the intestinal epithelium

Lucie Bernard-Raichon[1,2,3,4]*, Jessica A Neil[1,2,5]*, Kayla Kim[3], Thomas Heaney[1,2], Brittany M Miller[3], Damee Moon[2,6], Ashira Lubkin[2,7,8], Ashley L DuMont[2,9], Victor J Torres[2,9], Jordan Axelrad[10], Yu Matsuzawa-Ishimoto[1,2,11], and Ken Cadwell[1,2,3,12]

Affiliations:

1. Kimmel Center for Biology and Medicine at the Skirball Institute, New York University Grossman School of Medicine, New York, NY, USA.
2. Department of Microbiology, New York University Grossman School of Medicine, New York, NY, USA.
3. Division of Gastroenterology and Hepatology, Department of Medicine, University of Pennsylvania Perelman School of Medicine, Philadelphia, PA, USA.
4. Institut de Génomique Fonctionnelle de Lyon, École Normale Supérieure de Lyon, CNRS UMR 5242, UCBL Lyon-1, Lyon F-69007, France.
5. Department of Microbiology and Immunology, Peter Doherty Institute for Infection and Immunity, University of Melbourne, Melbourne, VIC, Australia
6. Institute for Systems Genetics, New York University Grossman School of Medicine, New York, New York, United States
7. Fungal Pathogenesis Section, Laboratory of Clinical Immunology and Microbiology, National Institute of Allergy and Infectious Diseases (NIAID), National Institutes of Health (NIH), Bethesda, MD, USA.
8. Postdoctoral Research Associate program, National Institute of General Medical Sciences, National Institutes of Health (NIH), Bethesda, MD, USA.
9. Department of Host-Microbe Interactions, St. Jude Children's Research Hospital, Memphis, TN, USA.
10. Division of Gastroenterology, Department of Medicine, NYU Grossman School of Medicine, New York, USA.

11. Department of Clinical and Diagnostic Laboratory Science Graduate School of Medical and Dental Science Institute of Science Tokyo (Science Tokyo), Tokyo, Japan
12. Department of Pathobiology, University of Pennsylvania School of Veterinary Medicine, Philadelphia, PA, USA.

* Authors contributed equally to this work

Correspondence:

Ken Cadwell: ken.cadwell@pennmedicine.upenn.edu, (215) 573-1076, 421 Curie Blvd, Philadelphia, PA 19104

Yu Matsuzawa-Ishimoto: matsuzawa.yu@tmd.ac.jp, +81-3-5803-5375, 1-5-45 Yushima, Bunkyo-ku, Tokyo,113-8510 Japan

Competing interests

K.C. has received research funding from Pfizer, Takeda, Pacific Biosciences, Genentech and Abbvie. K.C. has consulted for or received an honorarium for speaking engagement from Puretech Health, Genentech, Moderna, Gentibio, Pioneering Medicines, Prologue Medicines, and Abbvie. K.C. is an inventor on US patent 10,722,600 and provisional patent 63/157,225. J.A. has received research grants from BioFire Diagnostics, Genentech, Takeda, and Johnson & Johnson; consultancy fees, honorarium, or advisory board fees from Abbvie, Abviax, Adiso, BioFire Diagnostics, Biomerieux, Bristol-Myers Squibb, Celltrion, Ferring, Fresenius, Johnson & Johnson, Johnson & Johnson, Merck, Pfizer, Sanofi, Takeda, and Vedanta. V.J.T. is an inventor on patents and patent applications filed by New York University, which are currently under commercial license to Janssen Biotech Inc. Janssen Biotech Inc. provides research funding and other payments associated with the licensing agreement.

Abstract

Excessive cell death in the epithelium due to prolonged immune activation is associated with intestinal diseases such as Crohn's disease. Mice with mutations in the Crohn's disease susceptibility gene *Atg16l1* are susceptible to inflammation associated with intestinal epithelial cell (IEC) death, including loss of antimicrobial Paneth cells triggered by infection with murine norovirus (MNV). Here, we show that intestinal disease downstream of MNV depends on IFN-α/β and IFN-λ signaling in IECs. In mouse organoids, IFNs synergize with TNF to induce RIPK1-dependent cell death, amplified by ATG16L1 deficiency. We further show that human intestinal organoids harboring the *ATG16L1* risk allele exhibit heightened sensitivity to TNF and IFN co-stimulation and to serum from severe COVID-19 patients. Our findings reveal that virally triggered cytokines including IFNs exacerbate epithelial vulnerability in genetically predisposed hosts.

Keywords

Norovirus, interferons, autophagy, intestinal inflammation, necroptosis, Paneth cells.

71 **Introduction**

72 A single layer of epithelial cells in the intestine forms the first line of defense against
73 diverse microbial agents ranging from beneficial members of the microbiota to pathogens that
74 cause life-threatening disease[1]. Intestinal epithelial cells (IECs) include enterocytes that absorb
75 nutrients, chemosensory tuft cells, mucus-secreting goblet cells, and enteroendocrine cells that
76 produce hormones. The small intestinal crypt also harbors Paneth cells, IECs that secrete
77 antimicrobial factors such as lysozyme and defensins. The proper turnover of IECs maintains
78 anatomical integrity and contributes to resolving infections, such as through sloughing of
79 damaged or infected cells[2]. However, inflammatory or excessive cell death triggered by
80 prolonged immune activation is a hallmark of inflammatory bowel diseases (IBDs) such as
81 Crohn's disease (CD) and ulcerative colitis[3]. The cell death modality, timing, and cell type
82 specificity are likely important variables that contribute to outcomes in infectious and
83 inflammatory diseases of the gut.

84 The etiology of IBDs is complex and associated with genetic and environmental factors[4].
85 Although sustaining remission continues to be a challenge in many patients, the success of
86 therapies that target cytokines and their signaling activities support a disease model in which
87 these soluble immune mediators disrupt the epithelial barrier in a susceptible host. Consistent
88 with this possibility, we demonstrated that mutations in the CD susceptibility gene *ATG16L1* are
89 associated with loss of function and viability of Paneth cells as well as susceptibility to intestinal
90 injury downstream of TNF[5-8]. ATG16L1 is necessary for the cell biological process of autophagy
91 in which cytosolic material, such as protein aggregates and damaged organelles, is targeted to
92 the lysosome for degradation and recycling[9]. ATG16L1 and other autophagy genes have an
93 epithelial-intrinsic role in promoting intestinal barrier function[7, 10-16]. Autophagy and related
94 processes may be particularly important in Paneth cells because of their longevity (2-3 months)

95 and high secretory burden that make these cells susceptible to ER and mitochondrial stress[5, 7, 17, 18].

97 We previously developed a model in which *Atg16l1*-mutant mice, including mice with an IEC-specific deletion of *Atg16l1* (*Atg16l1*$^{fl/fl}$;villin-cre, hereafter referred to as *Atg16l1*$^{\Delta IEC}$), persistently infected with murine norovirus (MNV) are susceptible to chemical injury to the gut by dextran sodium sulfate (DSS) and develop Paneth cell alterations similar to those observed in patients with CD homozygous for the *ATG16L1 T300A* risk variant[6, 7]. Virally-triggered disease outcomes are dependent on TNF[6, 7]. This IEC-intrinsic role for ATG16L1 in mitigating damaged caused by TNF is reproduced in small intestinal organoids, a 3D cell culture model differentiated from intestinal stem cells. We and others showed that organoids generated from *Atg16l1*-mutant mice or patients with *ATG16L1*^{T300A} undergo necroptosis (programmed necrosis) and loss of Paneth cells upon TNF treatment[7, 13]. Given that MNV can promote beneficial immune development under certain settings and is otherwise tolerated[19-21], the virally-triggered intestinal damage observed in *Atg16l1*$^{\Delta IEC}$ mice provides an opportunity to identify the immune factors that regulate IEC-viability in response to environmental perturbations.

110 Type I Interferons (IFN-α/β) and type III interferons (IFN-λs) are best known for their antiviral functions downstream of Janus kinases (JAK) and signal transducer and activator of transcription proteins (STAT) upon receptor engagement. Although type I and III IFNs induce similar interferon stimulated genes (ISGs), they have distinct activities mediated in part by differential expression of their receptors. In the intestine, the type I IFN receptor (IFNAR) primarily functions in immune cells and is downregulated in IECs in adult mice whereas the type III IFN receptor (IFNLR) is highly expressed in IECs and neutrophils[22-24]. In the context of MNV infection, IFN-α/β prevents extraintestinal dissemination while IFN-λ restricts local replication and fecal shedding[25-29]. Although homeostatic IFN-λ produced by lymphocytes in response to commensal bacteria limits viral replication during early infection[30], the viral non-structural protein

120 NS1 encoded by persistent strains mediates evasion of IFN-λ to establish prolonged infection of
121 tuft cells[31, 32]. In addition to their antiviral role, IFNs impact intestinal homeostasis. A recent
122 study reported that mice lacking both IFNAR and IFNLR do not survive even low levels of DSS
123 exposure, which was associated with extensive destruction of the colonic epithelium[33]. By
124 contrast, IFN-λ levels are high in serum and small intestinal tissue of patients with CD, and over-
125 expression or administration of IFN-λ induces inflammatory forms of epithelial cell death,
126 necroptosis and pyroptosis[34, 35].

127 Although MNV can activate cell death proteins directly in infected IECs to promote its
128 reproduction and immune evasion[36-41], persistent strains display specific tropism for tuft cells
129 due to the restricted expression of the viral entry receptor *Cd300lf* [31, 42, 43]. Thus, in the *Atg16l1*
130 mutant setting, in which cell death is observed in Paneth cells that do not express *Cd300lf*,
131 extracellular factors mediate IEC defects. MNV increases TNF and IFN-γ producing intra-
132 epithelial lymphocytes and inhibits protective γδ T cells upstream of Paneth cell death and DSS-
133 induced disease[6-8]. Here, we identify a critical cytotoxic role of type I and III IFNs in mediating
134 these effects. We report that deletion of IFNAR or IFNLR in IECs rescues intestinal defects in
135 *Atg16l1* deficient mice and identify a role for IFNs in potentiating TNF-induced cell death. Using
136 organoids and serum from patients with COVID, we provide evidence that the general epithelial
137 cytotoxic effect of cytokines produced in response to viral infections is conserved in humans.
138 Thus, our results suggest that a component of viral sequelae includes production of soluble
139 immune mediators such as TNF and IFNs that compromise the viability of IECs, which is
140 especially detrimental in genetically susceptible hosts.

141

142

143

144 **Results**

145 *Epithelial type I and III interferon signaling mediate intestinal damage downstream of viral*
146 *infection.*

147 *Atg16l1*-mutant mice display spontaneous ISG expression in the gut dependent on the
148 microbiota[44, 45]. To determine whether ISG expression is further increased in the presence of
149 MNV, we examined the small intestine (ileum) and colon of WT and *Atg16l1*$^{\Delta IEC}$ mice 10 days
150 post intragastric infection with MNV strain CR6. The levels of three representative ISGs (*Mx2*,
151 *Oasl2*, and *Zbp1*) in the ileum and colon were increased by MNV infection, and for the ileum,
152 highest in MNV-infected *Atg16l1*$^{\Delta IEC}$ mice (Sup. Fig. 1A). IFN-λ is primarily responsible for ISG
153 expression in IECs[46]. To confirm that IFN-λ is responsible for the ISG expression, we crossed
154 *Ifnlr* floxed mice to *Atg16l1*$^{\Delta IEC}$ mice to obtain *Atg16l1;Ifnlr*$^{\Delta IEC}$ mice that are deficient in
155 ATG16L1 and IFNLR in IECs. ISG expression in MNV-infected *Atg16l1;Ifnlr*$^{\Delta IEC}$ mice was not
156 significantly different from uninfected Cre-negative controls, hereafter referred to as wild-type
157 (WT) (Sup. Fig. 1A).

158 To determine whether IFN-λ signaling contributes to virally triggered intestinal defects,
159 we examined the susceptibility of *Atg16l1;Ifnlr*$^{\Delta IEC}$ mice to DSS following MNV infection.
160 *Atg16l1*$^{\Delta IEC}$ mice showed increased lethality, weight loss, and disease score compared to WT
161 mice upon MNV + DSS treatment (Fig. 1A-C), similar to our previous study[7]. In contrast, these
162 disease signs were abrogated in MNV + DSS treated *Atg16l1;Ifnlr* $^{\Delta IEC}$ mice and were similar to
163 *Ifnlr*$^{\Delta IEC}$ (*Ifnlr*$^{fl/fl}$villin-cre) and WT controls (Fig. 1A-C). We also generated *Atg16l1;Ifnar*$^{\Delta IEC}$
164 (*Atg16l1*$^{fl/fl}$*Ifnar*$^{fl/fl}$villin-cre) mice for additional comparison and unexpectedly found that disease
165 was ameliorated. Consistent with a dominant antiviral role of IFNLR at the epithelial barrier
166 during MNV infection[26], *Atg16l1;Ifnlr*$^{\Delta IEC}$ mice, but not *Atg16l1;Ifnar*$^{\Delta IEC}$ mice, displayed
167 increased shedding of virus in stool compared to *Atg16l1*$^{\Delta IEC}$ or WT mice (Fig. 1D). None of the

168 mice examined displayed mortality or exacerbated disease in response to DSS in the absence
169 of MNV, except *Atg16l1;Ifnlr*$^{\Delta IEC}$ mice (Sup. Fig 1B). These results indicate that IFNLR and
170 IFNAR in IECs are necessary for the exacerbated intestinal injury response in *Atg16l1* $^{\Delta IEC}$ mice
171 infected with MNV and may have a different role in uninfected *Atg16l1* mutant mice.

172 We previously showed that Paneth cells are less frequent and structurally altered in the
173 ileum and that colons are shortened in MNV + DSS treated *Atg16l1*$^{\Delta IEC}$ mice[7]. *Atg16l1*$^{\Delta IEC}$ mice
174 also displayed a lower number of Paneth cells compared to similarly-treated WT mice, and the
175 remaining Paneth cells showed diffuse lysozyme staining and/or reduced number of lysozyme^{+}
176 granules that are a characteristic of CD[6]. Deleting *Ifnlr* or *Ifnar* in *Atg16l1* $^{\Delta IEC}$ mice led to partial
177 reversal of Paneth cell abnormalities. The number of Paneth cells in *Atg16l1;Ifnar*$^{\Delta IEC}$ mice were
178 increased compared to *Atg16l1*$^{\Delta IEC}$ mice and the proportion of abnormal Paneth cells were
179 reduced in *Atg16l1;Ifnlr*$^{\Delta IEC}$ mice (Fig. 1E-G). To test potential redundancy, we crossed
180 *Atg16l1;Ifnlr*$^{\Delta IEC}$ mice with *Atg16l1;Ifnar*$^{\Delta IEC}$ mice to generate *Atg16l1;Ifnlr;Ifnar* $^{\Delta IEC}$ mice deficient
181 in both receptors. However, *Atg16l1;Ifnlr;Ifnar* $^{\Delta IEC}$ mice still displayed reductions in Paneth cells
182 and a high proportion showed abnormal lysozyme staining compared with WT mice (Fig. 1E-G).
183 We cannot rule out the possibility that the above analyses would miss Paneth cells that lose
184 their granules, which can happen in the *Atg16l1* mutant setting[5]. To more broadly capture
185 abnormalities, we used terminal deoxynucleotidyl transferase–mediated dUTP nick-end labeling
186 (TUNEL) to detect cell death. TUNEL-positive cells were rarely detected in the crypts of WT
187 mice whereas a subset of crypts displayed multiple TUNEL-positive cells in *Atg16l1* $^{\Delta IEC}$ mice
188 (Fig. 1E, H). Rather than a decrease, the number of TUNEL-positive cells displayed a non-
189 significant increase in *Atg16l1;Ifnar* $^{\Delta IEC}$ mice compared with *Atg16l1* $^{\Delta IEC}$ mice. However, the
190 *Atg16l1;Ifnlr* $^{\Delta IEC}$ mice were similar to WT controls and *Atg16l1;Ifnlr;Ifnar* $^{\Delta IEC}$ mice were similar to
191 *Atg16l1* $^{\Delta IEC}$ mice (Fig. 1E, H). *Atg16l1*$^{\Delta IEC}$ mice also exhibited increased colon shortening
192 compared to WT and *Atg16l1;Ifnlr* $^{\Delta IEC}$ mice following MNV + DSS (Fig. 1I).

193 These results indicate that IFNLR and IFNAR signaling mediate lethality in MNV-infected
194 *Atg16l1*$^{\Delta IEC}$ mice. IFNLR and IFNAR contribute to Paneth cell abnormalities and cell death, but
195 deleting these receptors individually or together do not fully reverse these IEC defects.

196

197 *IFNβ and IFNλ exacerbate TNF-mediated cell death of intestinal organoids.*

198 We previously found that organoids generated from *Atg16l1*$^{\Delta IEC}$ mice (*Atg16l1*$^{-/-}$
199 organoids) display a striking spontaneous ISG signature and that treatment with the JAK
200 inhibitor ruxolitinib prevents TNF-induced cell death of these *Atg16l1*$^{-/-}$ organoids[10]. Although
201 these results are consistent with a role for signaling downstream of cytokine receptors that use
202 the JAK/STAT pathway, it was unclear whether IFNs can cooperate with TNF to induce loss of
203 organoid viability. Since the majority of *Atg16l1*$^{-/-}$ organoids die within the first 2-3 days of
204 seeding when TNF is administered on day 0[7], we modified our protocol to increase the dynamic
205 range of the assay and assess the synergistic effect of TNF and IFNs. We found that >50% of
206 *Atg16l1*$^{-/-}$ organoids and ~80% of *Atg16L1*$^{+/+}$ organoids (derived from *Atg16l1*$^{fl/fl}$ mice that were
207 negative for Cre) remained viable 72 hours post-stimulation when TNF was added 3 days after
208 seeding (Fig. 2A, B). Treatment with IFN-β and IFN-λ2 led to similar or slightly greater loss of
209 viability as TNF for both *Atg16L1*$^{+/+}$ and *Atg16l1*$^{-/-}$ organoids (Fig. 2A, B). In contrast, the
210 combination of TNF and IFN led to substantial organoid death. After only 24 h, *Atg16l1*$^{-/-}$
211 organoids stimulated with TNF + IFN-β or TNF + IFN-λ2 showed complete loss of viability (Fig.
212 2A, B). *Atg16L1*$^{+/+}$ organoids started to display loss of viability at 24 h and were completely dead
213 by 48-72 h post-treatment with TNF + IFN-β or TNF + IFN-λ2 (Fig. 2A, B). Titration of IFN-β and
214 IFN-λ2 in the presence of TNF showed dose responsiveness and that *Atg16l1*$^{-/-}$ organoids are
215 more sensitive to IFN since 10x less IFN induced same level of cell death in this genotype
216 compared with *Atg16L1*$^{+/+}$ organoids (Fig. 2C). Therefore, IFN-β and IFN-λ2 increase the toxicity

217 of TNF, and ATG16L1 deficiency further sensitizes organoids to the combination of these
218 cytokines.

219 IFN-β can induce TNF production[13], which may explain why IFN treatment alone can
220 induce some degree of cytotoxicity to organoids (Fig. 2B). We observed that *Tnf* gene
221 expression and protein secretion were increased in *Atg16l1*$^{-/-}$ organoids but not *Atg16L1*$^{+/+}$
222 organoids treated with IFN-β (Fig. 2D and Sup. Fig. 2A). Antibody-mediated blockade of TNF
223 rescued viability of *Atg16l1*$^{-/-}$ organoids stimulated with TNF as expected and also greatly
224 improved viability of *Atg16l1*$^{-/-}$ organoids treated with IFN-β (Fig. 2E). Anti-TNF improved
225 viability of *Atg16L1*$^{+/+}$ and *Atg16l1*$^{-/-}$ organoids treated with TNF + IFN-λ2 but not IFN-λ2 alone
226 (Sup. Fig. 2B). These results indicate that IFN-β increases the production of TNF in *Atg16l1*$^{-/-}$
227 organoids, which contributes to its toxicity.

228 We confirmed the specificity of IFN-β and IFN-λ2 for their cognate receptors. *Atg16l1*$^{-/-}$
229 *Ifnar*$^{-/-}$ organoids were resistant to TNF + IFN-β and *Atg16l1*$^{-/-}$*Ifnlr*$^{-/-}$ organoids were resistant to
230 TNF + IFN-λ2 (Fig. 2F). Also, IFN-β and IFN-λ2 did not induce representative ISGs in the
231 absence of their respective receptors (Sup. Fig. 2C). However, the spontaneous ISG expression
232 observed in untreated *Atg16l1*$^{-/-}$ organoids was absent in *Atg16l1*$^{-/-}$*Ifnlr*$^{-/-}$ but not *Atg16l1*$^{-/-}$*Ifnar*$^{-/-}$
233 organoids (Sup. Fig. 2C), suggesting a dominant role for IFNLR, possibly due to the
234 overexpression of *Ifnl2* in absence of IFNAR as previously described[47]. The necroptosis gene
235 *Mlkl* is also an ISG and displayed similar IFNAR and IFNLR dependent expression patterns
236 (Sup. Fig. 2C). Given our prior finding that ATG16L1-deficient organoids display spontaneous
237 ISG expression[10], we determined whether IFN receptor signaling contributed to cell death
238 induced by TNF alone. For these experiments, we added TNF to organoids on day 0, a
239 condition that allows us to examine toxicity of TNF treatment alone. Although the effect of
240 deleting IFNAR or IFNLR individually (*Atg16l1*$^{-/-}$*Ifnar*$^{-/-}$ and *Atg16l1*$^{-/-}$*Ifnlr*$^{-/-}$) was modest, deleting
241 both IFN receptors improved the viability of *Atg16l1*$^{-/-}$ organoids (*Atg16l1*$^{-/-}$*Ifnar*$^{-/-}$*Ifnlr*$^{-/-}$) (Fig. 2G).

242 When these experiments using exogenous cytokines and receptor deletions are taken together,
243 they show that IFNs synergize with TNF to mediate cell death, especially in the ATG16L1-
244 deficient setting.

245

246 *Exacerbation of TNF-induced toxicity in organoids by IFNs is partially dependent on necroptosis*
247 *signaling.*

248 TNF receptor engagement in IECs leads to activation of receptor-interacting
249 serine/threonine protein kinase 1 (RIPK1) to mediate either apoptosis or necroptosis in IECs[48,
250 49]. RIPK1 mediates apoptosis through caspases, and when apoptosis or caspases are inhibited,
251 necroptosis occurs through forming a complex with RIPK3 to phosphorylate the pore-forming
252 molecule MLKL that disrupts cell membrane integrity. We and others have shown that TNF-
253 induced cell death in *Atg16l1* deficient intestinal organoids and macrophages is dependent on
254 RIPK1, RIPK3, and MLKL[7, 13, 50]. To investigate how the combination of TNF and IFN reduced
255 viability, we treated organoids with ruxolitinib as a control, a pan-caspase inhibitor (QVD), and a
256 RIPK1-inhibitor (Nec1s). Ruxolitinib and Nec1s improved viability of both WT and *Atg16l1*-
257 deficient organoids treated with TNF + IFN-λ2 and TNF + IFN-β (Fig. 3A, B, Sup. Fig. 3A). By
258 contrast, QVD did not improve the viability of TNF + IFN stimulated organoids.

259 We first examined protein levels of cell death mediators at an early time point of cytokine
260 treatment before *Atg16l1*$^{-/-}$ organoids displayed signs of cytotoxicity. Even at 2 h post-
261 stimulation, phosphorylated RIPK3 (pRIPK3) and cleaved caspases, especially caspase-3, were
262 visible in TNF or TNF + IFN stimulated *Atg16l1*$^{-/-}$ organoids and not WT organoids (Fig. 3C-F,
263 Sup. Fig. 3B). This result is consistent with the delayed onset of cell death in WT organoids.
264 MLKL and cleaved caspase-3 were detected in WT organoids treated with IFN-λ2 for 24 h, with
265 or without TNF; pMLKL was faintly visible when both cytokines were present (Fig. 3F, G, Sup.

266 Fig. 3B). Although our earlier observation implicated necroptosis because RIPK1 inhibition and
267 not caspase inhibition protected organoids, we noted the prominent cleavage of caspase-3.
268 Therefore, we tested whether cell death induced by TNF and IFN treatment were dependent on
269 MLKL. *Mlkl*$^{-/-}$ organoids displayed increased viability when treated with TNF + IFN-λ2 or TNF +
270 IFN-β at 24 h, but this protection was less consistent at 48 h (Fig. 3I, H). These results indicate
271 that necroptosis contributes to the loss of viability induced by TNF + IFN treatment of organoids.

272 *Virally-triggered intestinal disease in Atg16l1 mutant mice is RIPK3-dependent.*

273 Paneth cell abnormalities and mortality are ameliorated by RIPK1 inhibition in MNV +
274 DSS-treated *Atg16l1*$^{\Delta IEC}$ mice[7]. As a kinase, RIPK3 may also be a targetable molecule. We
275 found that *Atg16l1*$^{\Delta IEC}$*;Ripk3*$^{-/-}$ mice showed substantially reduced lethality and weight loss
276 compared to *Atg16l1*$^{\Delta IEC}$ mice following MNV + DSS treatment similar to WT and *Ripk3*$^{-/-}$ control
277 mice (Fig. 4A). Although not a complete reversal, disease score and colon length of
278 *Atg16l1*$^{\Delta IEC}$*;Ripk3*$^{-/-}$ mice were not significantly different from WT and *Ripk3*$^{-/-}$ mice (Fig. 4A, B),
279 indicating a general improvement in disease outcomes. Additionally, Paneth cell numbers and
280 lysozyme staining were restored in *Atg16l1*$^{\Delta IEC}$*;Ripk3*$^{-/-}$ mice (Fig. 4C-E). These results show
281 that RIPK3 is necessary for susceptibility of *Atg16l1*$^{\Delta IEC}$ mice to MNV.

282

283 *Human organoids are susceptible to cell death induced by antiviral factors.*

284 The combination of TNF and IFNs is toxic to colonic organoids derived from humans,
285 although the concentration of cytokines necessary for cell death is high[51]. Based on our data
286 with mouse organoids, we hypothesized that human small intestinal organoids will be sensitive
287 to TNF + IFN treatment, especially in the presence of the *ATG16L1* risk allele. To test this
288 hypothesis, we utilized organoids that we previously generated from endoscopic biopsy

289 specimens that were genotyped for the *ATG16L1*^{T300A} variant (Sup Table 1)[10]. As in the mouse
290 model, the combination of TNF + IFN-λ2 induced cell death in human organoids, which was
291 exacerbated in those derived from individuals homozygous for *ATG16L1*^{T300A} (Fig. 5A-C).

292 TNF and IFNs are produced in response to most viral infections. We previously showed
293 that SARS-CoV-2 infected mice display a reduction in Paneth cell numbers and abnormal
294 lysozyme staining, reminiscent of *Atg16l1* mutant mice infected with MNV[52]. We did not detect
295 replication competent SARS-CoV-2 particles in the gut of these mice, raising the possibility that
296 circulating antiviral cytokines can mediate long-range cytotoxic effects on IECs in situations in
297 which they reach high levels, such as observed in severe COVID[53, 54]. Indeed, gastrointestinal
298 symptoms are common in patients with COVID-19 and many hospitalized patients display blood
299 stream infections (BSI) caused by microbes originating from the gut, suggesting intestinal
300 barrier defects[52]. To test whether soluble immune mediators associated with severe COVID-19
301 are cytotoxic to human IECs, we incubated the above organoids with serum samples pooled
302 from hospitalized patients during the height of the pandemic when individuals were screened for
303 SARS-CoV-2 infection. These samples were compared with serum from healthy volunteers and
304 hospitalized individuals who were COVID-negative but BSI-positive. Compared with serum from
305 healthy volunteers, addition of serum from patients with severe COVID led to increased loss of
306 viability, which was worse in organoids homozygous for *ATG16L1*^{T300A} (Fig. 5D-F). Serum from
307 BSI-positive control also worsened organoid death but not as severely as the COVID-positive
308 samples (Fig. 5 D-F). Therefore, circulating factors associated with severe COVID-19 display
309 cytotoxicity to IECs, and the *ATG16L1* risk variant further sensitizes cells to this activity.

310

311

312

313 **Discussion**

314 Our study demonstrates that type I and III IFNs are central mediators of intestinal
315 epithelial damage following viral infection in the context of ATG16L1 deficiency. Antiviral IFNs
316 and ISG expression have been observed in IBD patients but their contribution to the pathology
317 is incompletely understood[34, 55-57]. We show that IFN signaling in IECs drives epithelial cell death
318 and disease exacerbation in MNV-infected *Atg16l1*$^{\Delta IEC}$ mice, while organoid models reveal a
319 synergistic cytotoxicity between IFNs and TNF associated with necroptosis signaling. Notably,
320 deletion of IFN receptors rescued overall survival but had partial effects on Paneth cells. This
321 may reflect a confounding role for IFNs in controlling the virus, or alternatively, redundancy with
322 other cytokines such as IFN-γ, which is known to be upregulated during MNV infection and can
323 also trigger Paneth cell dysfunction[8, 58, 59]. IFN-γ and type I/III IFNs display redundancy in a
324 model of chronic murine astrovirus infection[60]. Also, the role of IFNAR was unexpected given
325 the dominance of IFNLR signaling in IECs and may reflect selective functions in a subset of
326 IECs or a role specific to the *Atg16l1* mutant setting. Future studies should explore whether
327 each IFN has a distinct IEC target and timing of activity that controls their cytotoxic effects.

328 These findings strengthen the link between infectious agents such as noroviruses and
329 CD[4, 61, 62]. Although noroviruses are associated with CD in some patients, they most often cause
330 self-resolving gastroenteritis and are detected in many asymptomatic individuals, suggesting
331 that as in our mouse model, the consequences of their presence depend on host factors and
332 may be immune mediated[63, 64]. A recent study showed that Epstein-Bar virus (EBV) infection
333 precedes CD[65]. Thus, triggers of intestinal inflammation are unlikely to be exclusive to
334 noroviruses but there may be some specificity. Although many types of gut microbes including
335 commensal bacteria evoke TNF and IFNs, our finding that serum from patients with severe
336 COVID-19 displays higher toxicity to organoids compared with serum from patients with non-
337 viral BSIs raises the possibility that certain types of infections are more likely to trigger

338 responses that cause IEC death. These observations also raise the intriguing possibility that
339 viral sequelae and chronic diseases like IBD share underlying mechanisms that include IEC
340 death. However, we acknowledge that our experimental system does not allow for such
341 comparisons, and that IBD is much more complex with a prolonged disease development and
342 cycles of healing and recurrence.

343 Therapeutically targeting signaling molecules upstream of cell death may offer a strategy
344 to protect the epithelium in at-risk individuals. Although RIPK3 deletion ameliorated disease in
345 *Atg16l1*$^{\Delta IEC}$ mice *in vivo*, RIPK1 inhibition may provide broader protection by blocking multiple
346 death pathways. Crosstalk between necroptosis, apoptosis, and pyroptosis and their co-
347 occurrence[66-68] may be especially relevant to organoids that harbor multiple IEC types. Our time
348 course experiments show that necroptosis inhibition delays but does not completely prevent
349 loss of viability in organoids. The partial rescue of viability is reminiscent of findings showing that
350 deleting *Tnfaip3* and *Tnip1* (genes that are also linked to IBD and autoimmunity) sensitizes to
351 TNF toxicity in the presence of microbial and viral ligands[69, 70]. Interventions that can be
352 personalized to restore function of a cell type that is specifically affected in a given susceptible
353 host, such as Paneth cells in the ATG16L1-deficient background, may be ideal. In this sense,
354 our observation that RIPK3 deletion better restores Paneth cells compared with IFN receptor
355 deletion supports targeting nodes at the intersection of multiple cytokine signaling pathways.
356 Indeed, clinically used JAK inhibitors effectively protect patient-derived colonic organoids from
357 cytokine cocktails[51].

358 In summary, this work positions IFNs as key players in virally triggered intestinal
359 pathology associated with TNF toxicity, particularly in the setting of ATG16L1 deficiency. It
360 underscores the need to consider synergistic cytokine responses in the management of CD and
361 other barrier-associated disorders.

362

363 **Methods**

364 *Mice*

365 Age- and gender-matched 8–12-week-old mice on the C57BL/6J (B6) background were used.
366 *Atg16l1*$^{f/f}$;VillinCre (*Atg16l1*$^{\Delta IEC}$) mice were provided by S. Virgin (Washington University School
367 of Medicine, St. Louis, MO) and crossed to *Ifnar1*$^{f/f}$ (Jax, 028256) and *Ifnlr1*$^{f/f}$ mice (provided by
368 S. Virgin) to obtain *Atg16l1;Ifnar*$^{\Delta IEC}$ and *Atg16l1;Ifnlr*$^{\Delta IEC}$ mice, respectively. To generate
369 littermate VillinCre-negative and *Atg16l1*$^{\Delta IEC}$ controls, mice were bred heterozygous for either
370 the *Ifnar*^{f} or *Ifnlr*^{f} genes and crossed VillinCre-positive with VillinCre-negative. Ifnar$^{\Delta IEC}$ and
371 *Ifnlr*$^{\Delta IEC}$ mice were bred separately by crossing VillinCre-positive with VillinCre-negative mice.
372 *Atg16l1;Ifnlr;Ifnar*$^{\Delta IEC}$ mice were obtained by crossing *Atg16l1;Ifnar1*$^{\Delta IEC}$ and *Atg16l1;Ifnlr*$^{\Delta IEC}$
373 mice. WT mice are a pool of VillinCre-negative mice from different crosses. *Rip3*$^{-/-}$ mice were
374 provided by G. Miller (NYU School of Medicine, New York, NY). *Mlkl*$^{-/-}$ mice were provided by J.
375 Murphy (WEHI, Parkville, Australia). All animal studies were performed according to approved
376 protocols by the New York University School of Medicine Institutional Animal Care and Use
377 Committees.

378 *MNV-triggered disease model*

379 MNV.CR6 stock was prepared as previously described and as detailed in the Supplementary
380 method section[71]. Mice were infected orally with 3×10^6 PFUs resuspended in PBS. Viral
381 burden in stool at day 10 post infection was determined by plaque assay. On day 10 post-
382 infection, mice were administered 5% Dextran Sulfate Sodium (DSS) (TdB Consultancy) in their
383 drinking water for 6 d after which it was replaced by regular drinking water. *Ripk3*$^{-/-}$ mice showed
384 increased lethality when given 5% DSS. When these mice were used, 3% DSS was used
385 instead of 5% as indicated in the figure legend. Clinical disease score and mouse weight were
386 assessed daily. Disease score was quantified on the basis of five parameters as described

387 previously, including diarrhea (0–2), hunched posture (0–2), fur ruffling (0 or 1), mobility (0–2),
388 and blood stool (0 or 1), in which 8 was the maximum score for the pathology[7]. For survival
389 experiments, mice were euthanized if they reached the humane end point. In other experiments,
390 mice were sacrificed before receiving DSS or after receiving 5 days of DSS (which occurred
391 before clinical disease signs).

392 *Intestinal organoid culture*

393 Murine and human organoids (generated during previous studies[10, 72]) were cultured as
394 described in the Supplementary methods. Murine organoids were treated with 20 ng/ml mTNFα
395 (Peprotech) and indicated concentrations of mIFNβ (PBL assay science) and mIFNλ2
396 (Peprotech). In some experiments, organoids were pre-treated with 100nM Ruxolitinib, 10μM Q-
397 VD-OPh (Millipore Sigma), 10 μM Necrostatin-1s (Nec-1s) (Biovision), 20 μg/ml anti-TNFα
398 antibody (XT3.11, BioXcell) or 20 μg/ml Rat IgG1 isotype control (HRPN, BioXcell). Human
399 organoids were treated with 50 ng/mL hTNFα (Peprotech), 100 ng/mL hIFNλ2 (R&D systems).
400 In another experiment, half of the DMEM/F-12 in the differentiation medium was replaced by
401 human serum (growth factors were maintained at same concentrations). Serum from healthy
402 donors from the United States was purchased from SeraCare. The serum from patients with BSI
403 and SARS-CoV-2 infection was collected at the NYU Langone hospital in 2020 during a
404 previous study (Table S3)[73]. Each organoid donor was stimulated with the same pool of serum
405 obtained from healthy donors, patients with BSI and negative for SARS-CoV-2 by qPCR or with
406 BSI and positive for SARS-CoV-2. Percentages of viable organoids were determined based on
407 morphology by daily quantification as before[7]. Dead organoids were also marked by staining
408 with 100 μg/ml PI (Sigma-Aldrich) and 100 μg/ml Hoechst 33342 (Invitrogen) to confirm
409 phenotypes.

410

411 *Statistical analysis*

412 GraphPad Prism version 10 was used for statistical analysis unless otherwise specified.
413 Survival data were analyzed by Kaplan-Meier with Log-rank test followed by Holm Sidak's
414 multiple comparison test (Figure 1A, 4A). For other parameters, ordinary or lognormal ordinary
415 (PFU, Figure 1D) one-way ANOVA and Tukey's multiple comparison were used when data
416 followed a normal distribution or a Kruskal-Wallis test followed by Dunn's multiple comparison
417 test when they did not (disease score, Figure 1B). For histological measurements, the effect of
418 mouse genotype was determined on R using individual measurements (e.g. number of Paneth
419 cells in 50 crypts per mouse) while adjusting for batch effect caused by individual mouse and
420 experiments. ANOVA type III followed by Tukey's multiple comparison Generalized Linear
421 Mixed Model (GLMM) was used for Paneth cell counts. A beta-binomial analysis followed by
422 Tukey's multiple comparison was used for Paneth cell abnormality. Negative Binomial GLMM
423 was used to compare the number of TUNEL+ cells per crypt.
424 In Figure 2 and 3, in each experiment, organoids derived from a single mouse per genotype
425 were stimulated with different cytokines and inhibitors (experiments were then repeated in
426 independent experiments using organoids derived from different mice). Ordinary one-way
427 ANOVA were used to compare the effect of the treatment within a genotype, two-way ANOVA
428 were used when comparing the effect of the treatment and of the genotypes, followed by
429 Sidak's multiple comparison test. Comparison of area under the curve was performed to
430 compare time-course curves. For human organoids, an ANOVA followed by Sidak's multiple
431 comparison test was used to compare the effect of the stimulation on organoid viability
432 depending on the genotype.

433

434

435 **Data availability**

436 All data generated or analysed during this study are included in this published article and its
437 supplementary information files.

438 **Acknowledgements**

439 We thank the NYU Langone's Experimental Pathology Research Laboratory
440 (RRID:SCR_017928) and the NYU Langone's Microscopy Laboratory (RRID: SCR_017934),
441 supported in part by NYU Langone Health's Laura and Isaac Perlmutter Cancer Center Support
442 (grant P30CA016087), for the use of their instruments and technical assistance. We thank the
443 following University of Pennsylvania core facilities for their expert technical support: the Cell and
444 Developmental Biology (CDB) Microscopy Core (RRID SCR_022373) as well as the Molecular
445 Pathology & Imaging Core (MPIC) (RRID: SCR_022420) and Genetically Engineered Mouse
446 Core supported by the UPENN Digestive and Liver Center (P30DK050306). We also thank M.
447 B. da Silva, Y. Shono and M. R. M. van den Brink for their support with TUNEL staining and N
448 Desvignes and A Lambert for their help with lysozyme staining. We also thank Filipe De Vadder
449 for his kind help with statistical analyses. This research was funded in part by NIH grants
450 DK093668 (K.C.), AI121244 (K.C.), AI140754 (K.C.), AI179896 (K.C.), and DK050306 (K.C.);
451 Shanahan Family Fund for Inflammatory Bowel Disease Research (K.C.); pilot grant from King
452 Center for Lynch Syndrome (K.C.); pilot grant from Abramson Cancer Center (K.C.); and an
453 industry partnership with AbbVie Inc. (K.C.).

454 **Author contributions**

455 LBR, JAN, YMI and KC designed the study. LBR, JAN and YMI performed most of the
456 experiments with assistance from KK, TH, and DM and BMM. YMI and JA provided the human
457 organoids lines. AL, AD and VJT provided the human serum samples. LBR, JAN and KC

458 drafted the manuscript. All authors contributed to refinement of the study protocol and approved
459 the final manuscript.

460

461

462

463

464

465

466

467 **References**

468 1. Ramanan D, Cadwell K. Intrinsic Defense Mechanisms of the Intestinal Epithelium. *Cell Host*
469 *Microbe* 2016; **19**(4)**:** 434-441.

470

471 2. Churchill MJ, Mitchell PS, Rauch I. Epithelial Pyroptosis in Host Defense. *J Mol Biol* 2022; **434**(4)**:**
472 167278.

473

474 3. Patankar JV, Becker C. Cell death in the gut epithelium and implications for chronic
475 inflammation. *Nat Rev Gastroenterol Hepatol* 2020; **17**(9)**:** 543-556.

476

477 4. Cadwell K, Loke P. Gene-environment interactions shape the host-microbial interface in
478 inflammatory bowel disease. *Nat Immunol* 2025; **26**(7)**:** 1023-1035.

479

480 5. Cadwell K, Liu JY, Brown SL, Miyoshi H, Loh J, Lennerz JK *et al.* A key role for autophagy and the
481 autophagy gene Atg16l1 in mouse and human intestinal Paneth cells. *Nature* 2008; **456**(7219)**:**
482 259-263.

483

484 6. Cadwell K, Patel KK, Maloney NS, Liu TC, Ng AC, Storer CE *et al.* Virus-plus-susceptibility gene
485 interaction determines Crohn's disease gene Atg16L1 phenotypes in intestine. *Cell* 2010; **141**(7)**:**
486 1135-1145.

487

488 7. Matsuzawa-Ishimoto Y, Shono Y, Gomez LE, Hubbard-Lucey VM, Cammer M, Neil J *et al.*
489 Autophagy protein ATG16L1 prevents necroptosis in the intestinal epithelium. *J Exp Med* 2017;
490 **214**(12)**:** 3687-3705.

491

492 8. Matsuzawa-Ishimoto Y, Yao X, Koide A, Ueberheide BM, Axelrad JE, Reis BS *et al.* The
493 gammadelta IEL effector API5 masks genetic susceptibility to Paneth cell death. *Nature* 2022;
494 **610**(7932)**:** 547-554.

495

496 9. Matsuzawa-Ishimoto Y, Hwang S, Cadwell K. Autophagy and Inflammation. *Annu Rev Immunol*
497 2018; **36:** 73-101.

498

499 10. Matsuzawa-Ishimoto Y, Hine A, Shono Y, Rudensky E, Lazrak A, Yeung F *et al.* An intestinal
500 organoid-based platform that recreates susceptibility to T-cell-mediated tissue injury. *Blood*
501 2020; **135**(26)**:** 2388-2401.

502

503 11. Jackson DN, Panopoulos M, Neumann WL, Turner K, Cantarel BL, Thompson-Snipes L *et al.*
504 Mitochondrial dysfunction during loss of prohibitin 1 triggers Paneth cell defects and ileitis. *Gut*
505 2020; **69**(11)**:** 1928-1938.

506
507 12. Foerster EG, Tsang DKL, Goyal S, Robertson SJ, Robert LM, Maughan H *et al.* ATG16L1 protects
508 from interferon-gamma-induced cell death in the small intestinal crypt. *Mucosal Immunol* 2023;
509 **16**(2)**:** 135-152.

510
511 13. Aden K, Tran F, Ito G, Sheibani-Tezerji R, Lipinski S, Kuiper JW *et al.* ATG16L1 orchestrates
512 interleukin-22 signaling in the intestinal epithelium via cGAS-STING. *J Exp Med* 2018; **215**(11)**:**
513 2868-2886.

514
515 14. Pott J, Kabat AM, Maloy KJ. Intestinal Epithelial Cell Autophagy Is Required to Protect against
516 TNF-Induced Apoptosis during Chronic Colitis in Mice. *Cell Host Microbe* 2018; **23**(2)**:** 191-202
517 e194.

518
519 15. Jung H, Leal-Ekman JS, Lu Q, Stappenbeck TS. Atg14 protects the intestinal epithelium from TNF-
520 triggered villus atrophy. *Autophagy* 2019; **15**(11)**:** 1990-2001.

521
522 16. Asano J, Sato T, Ichinose S, Kajita M, Onai N, Shimizu S *et al.* Intrinsic Autophagy Is Required for
523 the Maintenance of Intestinal Stem Cells and for Irradiation-Induced Intestinal Regeneration.
524 *Cell Rep* 2017; **20**(5)**:** 1050-1060.

525
526 17. Bel S, Pendse M, Wang Y, Li Y, Ruhn KA, Hassell B *et al.* Paneth cells secrete lysozyme via
527 secretory autophagy during bacterial infection of the intestine. *Science* 2017; **357**(6355)**:** 1047-
528 1052.

529
530 18. Adolph TE, Tomczak MF, Niederreiter L, Ko HJ, Bock J, Martinez-Naves E *et al.* Paneth cells as a
531 site of origin for intestinal inflammation. *Nature* 2013; **503**(7475)**:** 272-276.

532
533 19. Kernbauer E, Ding Y, Cadwell K. An enteric virus can replace the beneficial function of
534 commensal bacteria. *Nature* 2014; **516**(7529)**:** 94-98.

535
536 20. Neil JA, Matsuzawa-Ishimoto Y, Kernbauer-Holzl E, Schuster SL, Sota S, Venzon M *et al.* IFN-I and
537 IL-22 mediate protective effects of intestinal viral infection. *Nat Microbiol* 2019; **4**(10)**:** 1737-
538 1749.

539
540 21. Abt MC, Buffie CG, Susac B, Becattini S, Carter RA, Leiner I *et al.* TLR-7 activation enhances IL-22-
541 mediated colonization resistance against vancomycin-resistant enterococcus. *Sci Transl Med*
542 2016; **8**(327)**:** 327ra325.

543
544 22. Ingle H, Peterson ST, Baldridge MT. Distinct Effects of Type I and III Interferons on Enteric
545 Viruses. *Viruses* 2018; **10**(1).

546

547 23. Lin JD, Feng N, Sen A, Balan M, Tseng HC, McElrath C *et al.* Distinct Roles of Type I and Type III
548 Interferons in Intestinal Immunity to Homologous and Heterologous Rotavirus Infections. *PLoS*
549 *Pathog* 2016; **12**(4)**:** e1005600.

550

551 24. Mahlakoiv T, Hernandez P, Gronke K, Diefenbach A, Staeheli P. Leukocyte-derived IFN-
552 alpha/beta and epithelial IFN-lambda constitute a compartmentalized mucosal defense system
553 that restricts enteric virus infections. *PLoS Pathog* 2015; **11**(4)**:** e1004782.

554

555 25. Rocha-Pereira J, Jacobs S, Noppen S, Verbeken E, Michiels T, Neyts J. Interferon lambda (IFN-
556 lambda) efficiently blocks norovirus transmission in a mouse model. *Antiviral Res* 2018; **149:** 7-
557 15.

558

559 26. Nice TJ, Baldridge MT, McCune BT, Norman JM, Lazear HM, Artyomov M *et al.* Interferon-
560 lambda cures persistent murine norovirus infection in the absence of adaptive immunity.
561 *Science* 2015; **347**(6219)**:** 269-273.

562

563 27. Thackray LB, Duan E, Lazear HM, Kambal A, Schreiber RD, Diamond MS *et al.* Critical role for
564 interferon regulatory factor 3 (IRF-3) and IRF-7 in type I interferon-mediated control of murine
565 norovirus replication. *J Virol* 2012; **86**(24)**:** 13515-13523.

566

567 28. Baldridge MT, Lee S, Brown JJ, McAllister N, Urbanek K, Dermody TS *et al.* Expression of Ifnlr1 on
568 Intestinal Epithelial Cells Is Critical to the Antiviral Effects of Interferon Lambda against
569 Norovirus and Reovirus. *J Virol* 2017; **91**(7).

570

571 29. Nice TJ, Osborne LC, Tomov VT, Artis D, Wherry EJ, Virgin HW. Type I Interferon Receptor
572 Deficiency in Dendritic Cells Facilitates Systemic Murine Norovirus Persistence Despite Enhanced
573 Adaptive Immunity. *PLoS Pathog* 2016; **12**(6)**:** e1005684.

574

575 30. Van Winkle JA, Peterson ST, Kennedy EA, Wheadon MJ, Ingle H, Desai C *et al.* Homeostatic
576 interferon-lambda response to bacterial microbiota stimulates preemptive antiviral defense
577 within discrete pockets of intestinal epithelium. *Elife* 2022; **11**.

578

579 31. Wilen CB, Lee S, Hsieh LL, Orchard RC, Desai C, Hykes BL, Jr. *et al.* Tropism for tuft cells
580 determines immune promotion of norovirus pathogenesis. *Science* 2018; **360**(6385)**:** 204-208.

581

582 32. Lee S, Wilen CB, Orvedahl A, McCune BT, Kim KW, Orchard RC *et al.* Norovirus Cell Tropism Is
583 Determined by Combinatorial Action of a Viral Non-structural Protein and Host Cytokine. *Cell*
584 *Host Microbe* 2017; **22**(4)**:** 449-459 e444.

585

586 33. McElrath C, Espinosa V, Lin JD, Peng J, Sridhar R, Dutta O *et al.* Critical role of interferons in
587 gastrointestinal injury repair. *Nat Commun* 2021; **12**(1)**:** 2624.

588
589 34. Gunther C, Ruder B, Stolzer I, Dorner H, He GW, Chiriac MT *et al.* Interferon Lambda Promotes
590 Paneth Cell Death Via STAT1 Signaling in Mice and Is Increased in Inflamed Ileal Tissues of
591 Patients With Crohn's Disease. *Gastroenterology* 2019; **157**(5)**:** 1310-1322 e1313.

592
593 35. Jena KK, Mambu J, Boehmer D, Sposito B, Millet V, de Sousa Casal J *et al.* Type III interferons
594 induce pyroptosis in gut epithelial cells and impair mucosal repair. *Cell* 2024; **187**(26)**:** 7533-
595 7550 e7523.

596
597 36. Robinson BA, Van Winkle JA, McCune BT, Peters AM, Nice TJ. Caspase-mediated cleavage of
598 murine norovirus NS1/2 potentiates apoptosis and is required for persistent infection of
599 intestinal epithelial cells. *PLoS Pathog* 2019; **15**(7)**:** e1007940.

600
601 37. Wang G, Zhang D, Orchard RC, Hancks DC, Reese TA. Norovirus MLKL-like protein initiates cell
602 death to induce viral egress. *Nature* 2023; **616**(7955)**:** 152-158.

603
604 38. Song J, Zhang L, Moon S, Fang A, Wang G, Gheshm N *et al.* Norovirus co-opts NINJ1 for selective
605 protein secretion. *Sci Adv* 2025; **11**(9)**:** eadu7985.

606
607 39. Deerain JM, Aktepe TE, Trenerry AM, Ebert G, Hyde JL, Charry K *et al.* Murine norovirus infection
608 of macrophages induces intrinsic apoptosis as the major form of programmed cell death.
609 *Virology* 2024; **589:** 109921.

610
611 40. Bok K, Prikhodko VG, Green KY, Sosnovtsev SV. Apoptosis in murine norovirus-infected
612 RAW264.7 cells is associated with downregulation of survivin. *J Virol* 2009; **83**(8)**:** 3647-3656.

613
614 41. Aktepe TE, Deerain JM, Hyde JL, Fritzlar S, Mead EM, Carrera Montoya J *et al.* Norovirus-
615 mediated translation repression promotes macrophage cell death. *PLoS Pathog* 2024; **20**(9)**:**
616 e1012480.

617
618 42. Orchard RC, Wilen CB, Doench JG, Baldridge MT, McCune BT, Lee YC *et al.* Discovery of a
619 proteinaceous cellular receptor for a norovirus. *Science* 2016; **353**(6302)**:** 933-936.

620
621 43. Graziano VR, Alfajaro MM, Schmitz CO, Filler RB, Strine MS, Wei J *et al.* CD300lf Conditional
622 Knockout Mouse Reveals Strain-Specific Cellular Tropism of Murine Norovirus. *J Virol* 2021;
623 **95**(3).

624
625 44. Martin PK, Marchiando A, Xu R, Rudensky E, Yeung F, Schuster SL *et al.* Autophagy proteins
626 suppress protective type I interferon signalling in response to the murine gut microbiota. *Nat*
627 *Microbiol* 2018; **3**(10)**:** 1131-1141.

628

629 45. Marchiando AM, Ramanan D, Ding Y, Gomez LE, Hubbard-Lucey VM, Maurer K *et al.* A deficiency
630 in the autophagy gene Atg16L1 enhances resistance to enteric bacterial infection. *Cell Host*
631 *Microbe* 2013; **14**(2)**:** 216-224.

632

633 46. Odendall C, Dixit E, Stavru F, Bierne H, Franz KM, Durbin AF *et al.* Diverse intracellular pathogens
634 activate type III interferon expression from peroxisomes. *Nat Immunol* 2014; **15**(8)**:** 717-726.

635

636 47. Ardanuy J, Scanlon K, Skerry C, Fuchs SY, Carbonetti NH. Age-Dependent Effects of Type I and
637 Type III IFNs in the Pathogenesis of Bordetella pertussis Infection and Disease. *J Immunol* 2020;
638 **204**(8)**:** 2192-2202.

639

640 48. Dannappel M, Vlantis K, Kumari S, Polykratis A, Kim C, Wachsmuth L *et al.* RIPK1 maintains
641 epithelial homeostasis by inhibiting apoptosis and necroptosis. *Nature* 2014; **513**(7516)**:** 90-94.

642

643 49. Kattah MG, Shao L, Rosli YY, Shimizu H, Whang MI, Advincula R *et al.* A20 and ABIN-1
644 synergistically preserve intestinal epithelial cell survival. *J Exp Med* 2018; **215**(7)**:** 1839-1852.

645

646 50. Lim J, Park H, Heisler J, Maculins T, Roose-Girma M, Xu M *et al.* Autophagy regulates
647 inflammatory programmed cell death via turnover of RHIM-domain proteins. *Elife* 2019; **8**.

648

649 51. Jang KK, Hudesman D, Jones DR, Loke P, Axelrad JE, Cadwell K *et al.* Tofacitinib Uptake by
650 Patient-Derived Intestinal Organoids Predicts Individual Clinical Responsiveness.
651 *Gastroenterology* 2024; **167**(7)**:** 1453-1456 e1455.

652

653 52. Bernard-Raichon L, Venzon M, Klein J, Axelrad JE, Zhang C, Sullivan AP *et al.* Gut microbiome
654 dysbiosis in antibiotic-treated COVID-19 patients is associated with microbial translocation and
655 bacteremia. *Nat Commun* 2022; **13**(1)**:** 5926.

656

657 53. Ghaffarpour S, Ghazanfari T, Ardestani SK, Naghizadeh MM, Vaez Mahdavi MR, Salehi M *et al.*
658 Cytokine profiles dynamics in COVID-19 patients: a longitudinal analysis of disease severity and
659 outcomes. *Sci Rep* 2025; **15**(1)**:** 14209.

660

661 54. Araujo R, Von Rekowski CP, Fonseca TAH, Calado CRC, Ramalhete L, Bento L. Multiplex Targeted
662 Proteomic Analysis of Cytokine Ratios for ICU Mortality in Severe COVID-19. *Proteomes* 2025;
663 **13**(3).

664

665 55. Mavragani CP, Nezos A, Dovrolis N, Andreou NP, Legaki E, Sechi LA *et al.* Type I and II Interferon
666 Signatures Can Predict the Response to Anti-TNF Agents in Inflammatory Bowel Disease
667 Patients: Involvement of the Microbiota. *Inflamm Bowel Dis* 2020; **26**(10)**:** 1543-1553.

668

669 56. Veyssiere M, Hammoudi N, Le Bourhis L, Hassid D, Bonnet J, Tran Minh ML *et al.* Blood
670 proteomic signatures associated with disease activity in inflammatory bowel diseases. *J Crohns*
671 *Colitis* 2025; **19**(9).

672

673 57. Ostvik AE, Svendsen TD, Granlund AVB, Doseth B, Skovdahl HK, Bakke I *et al.* Intestinal Epithelial
674 Cells Express Immunomodulatory ISG15 During Active Ulcerative Colitis and Crohn's Disease. *J*
675 *Crohns Colitis* 2020; **14**(7)**:** 920-934.

676

677 58. Farin HF, Karthaus WR, Kujala P, Rakhshandehroo M, Schwank G, Vries RG *et al.* Paneth cell
678 extrusion and release of antimicrobial products is directly controlled by immune cell-derived
679 IFN-gamma. *J Exp Med* 2014; **211**(7)**:** 1393-1405.

680

681 59. Tomov VT, Palko O, Lau CW, Pattekar A, Sun Y, Tacheva R *et al.* Differentiation and Protective
682 Capacity of Virus-Specific CD8(+) T Cells Suggest Murine Norovirus Persistence in an Immune-
683 Privileged Enteric Niche. *Immunity* 2017; **47**(4)**:** 723-738 e725.

684

685 60. Herrmann C, Zaldana K, Lustig AM, Bee GCW, Agostino EL, Koralov SB *et al.* Environmental stress
686 drives clearance of a persistent enteric virus in mice. *Nat Microbiol* 2025; **10**(8)**:** 1975-1988.

687

688 61. Axelrad JE, Chen Z, Devlin J, Ruggles KV, Cadwell K. Pathogen-Specific Alterations in the Gut
689 Microbiota Predict Outcomes in Flare of Inflammatory Bowel Disease Complicated by
690 Gastrointestinal Infection. *Clin Transl Gastroenterol* 2023; **14**(2)**:** e00550.

691

692 62. Axelrad JE, Olen O, Askling J, Lebwohl B, Khalili H, Sachs MC *et al.* Gastrointestinal Infection
693 Increases Odds of Inflammatory Bowel Disease in a Nationwide Case-Control Study. *Clin*
694 *Gastroenterol Hepatol* 2019; **17**(7)**:** 1311-1322 e1317.

695

696 63. Bernard-Raichon L, Cadwell K. Immunomodulation by Enteric Viruses. *Annu Rev Virol* 2023;
697 **10**(1)**:** 477-502.

698

699 64. Lindesmith LC, Donaldson EF, Lobue AD, Cannon JL, Zheng DP, Vinje J *et al.* Mechanisms of GII.4
700 norovirus persistence in human populations. *PLoS Med* 2008; **5**(2)**:** e31.

701

702 65. Nandy A, Petralia F, Porter CK, Elledge S, Viruses, Group IBDS *et al.* Epstein-Barr Virus Exposure
703 Precedes Crohn's Disease Development. *Gastroenterology* 2025; **169**(1)**:** 150-153.

704

705 66. Araujo A, Safronova A, Burger E, Lopez-Yglesias A, Giri S, Camanzo ET *et al.* IFN-gamma mediates
706 Paneth cell death via suppression of mTOR. *Elife* 2021; **10**.

707

708 67. Newton K, Dugger DL, Wickliffe KE, Kapoor N, de Almagro MC, Vucic D *et al.* Activity of protein
709 kinase RIPK3 determines whether cells die by necroptosis or apoptosis. *Science* 2014; **343**(6177)**:**
710 1357-1360.

711
712 68. Malireddi RKS, Kanneganti TD. Three decades of caspases and RIPKs in life and death. *Hum Mol*
713 *Genet* 2025; **34**(R1)**:** R121-R136.

714
715 69. Su Z, Dziedzic SA, Hu D, Barrett VJ, Broekema N, Li W *et al.* ABIN-1 heterozygosity sensitizes to
716 innate immune response in both RIPK1-dependent and RIPK1-independent manner. *Cell Death*
717 *Differ* 2019; **26**(6)**:** 1077-1088.

718
719 70. Rusu I, Mennillo E, Bain JL, Li Z, Sun X, Ly KM *et al.* Microbial signals, MyD88, and lymphotoxin
720 drive TNF-independent intestinal epithelial tissue damage. *J Clin Invest* 2022; **132**(5).

721
722 71. Strong DW, Thackray LB, Smith TJ, Virgin HW. Protruding domain of capsid protein is necessary
723 and sufficient to determine murine norovirus replication and pathogenesis in vivo. *J Virol* 2012;
724 **86**(6)**:** 2950-2958.

725
726 72. Jang KK, Kaczmarek ME, Dallari S, Chen YH, Tada T, Axelrad J *et al.* Variable susceptibility of
727 intestinal organoid-derived monolayers to SARS-CoV-2 infection. *PLoS Biol* 2022; **20**(3)**:**
728 e3001592.

729
730 73. Lubkin A, Bernard-Raichon L, DuMont AL, Valero Jimenez AM, Putzel GG, Gago J *et al.* SARS-CoV-
731 2 infection predisposes patients to coinfection with Staphylococcus aureus. *mBio* 2024; **15**(8)**:**
732 e0166724.

733

734

735

736

737 **Figure legends**

738 **Figure 1:** ***Epithelial type I and III interferon signaling mediate intestinal damage***
739 ***downstream of viral infection.*** **(A)** Survival of wildtype (WT; villin-cre^{-} littermate controls),
740 *Atg16l1*$^{\Delta IEC}$, *Atg16l1;Ifnlr*$^{\Delta IEC}$, *Ifnlr*$^{\Delta IEC}$, *Atg16l1;Ifnar*$^{\Delta IEC}$, and *Ifnar*$^{\Delta IEC}$ mice receiving 5% DSS in
741 drinking water for 6 days starting 10 days post inoculation (dpi) with MNV. **(B-C)** Cumulative
742 disease score (B) and weight loss (C) at day 6 post DSS from mice in (A). **(D)** Plaque forming
743 units (PFUs) of MNV per gram of stool from mice in (A) at 10 dpi. **(E-F)** Representative images
744 of ileal crypts stained for lysozyme (red) and DAPI (blue) (top) or for deoxynucleotidyl
745 transferase–mediated dUTP nick-end labeling (TUNEL) (bottom) of WT, *Atg16l1*$^{\Delta IEC}$,
746 *Atg16l1;Ifnar*$^{\Delta IEC}$, *Atg16l1;Ifnlr*$^{\Delta IEC}$, and *Atg16l1;Ifnlr;Ifnar*$^{\Delta IEC}$ mice infected with MNV on day 5
747 post DSS treatment as in (A) (scale bars 20μm). **(F)** Violin plots depicting the repartition of the
748 number of Paneth cells observed in individual crypts, overlayed with symbols representing the
749 average number of Paneth cells per crypt observed in each mouse based on the lysozyme
750 staining shown in (E). **(G)** Average proportion of abnormal Paneth cells per crypt observed in
751 each mouse as determined on the basis of whether each Paneth cell displayed a typical staining
752 pattern with distinguishable granules (normal, orange arrow) or depleted and/or diffuse
753 lysozyme staining (abnormal, white arrow) as indicated in (E). **(H)** Proportion of crypts with 1, 2
754 or 3-5 TUNEL+ cells per mouse of each genotype. Orange arrowheads indicate TUNEL^{+} cells in
755 (E). At least 50 villi and crypts were quantified per mouse. **(I)** Measurement of colon length from
756 mice in (E-H). Each symbol represents individual mice (or the mean in A) with bars representing
757 mean ± SEM from at least two independent experiments. Comparison between all genotypes
758 was performed, not significant comparisons are not indicated, *p≤0.05, **p≤0.01, ***p≤0.001,
759 ****p≤0.0001, See also Figure S1.

760

761 **Figure 2: IFNβ and IFNλ2 exacerbate TNF-mediated cell death of intestinal organoids. (A)**
762 Representative images of small intestinal organoids derived from WT (*Atg16l1*$^{+/+}$)
763 and *Atg16l1*$^{\Delta IEC}$ mice (*Atg16l1*$^{-/-}$) cultivated in ENR medium for 3 days and stimulated for another
764 24h ± 20 ng/ml TNF, ± 100 U/ml IFNβ and ± 1ng/ml IFNλ2, then stained with Hoechst (blue) for
765 nuclei and propidium iodide (PI) (red) for cell death. Scale bars represent 1000 μm. **(B)** Viability
766 of *Atg16l1*$^{+/+}$ and *Atg16l1*$^{-/-}$ organoids stimulated with indicated cytokines over time as
767 determined by PI staining and organoid morphology. **(C)** Viability of organoids 48h post
768 stimulation with 20 ng/ml TNF and 1 (low), 10 (med), 100 (high) U/ml IFNβ (left panel) or 0.01
769 (low), 0.1 (med), 1 (high) ng/ml IFNλ2 (right panel). **(D)** Quantification of TNF in culture
770 supernatants by ELISA from indicated organoids stimulated or not with 100 U/ml IFNβ for 48h.
771 **(E)** Viability of *Atg16l1*$^{+/+}$ (left) or *Atg16l1*$^{-/-}$ (right) organoids treated with 20 µg/ml anti-TNFα
772 antibody or isotype control for at least 30min before stimulation with cytokines. **(F)** Viability of
773 *Atg16l1*$^{+/+}$, *Atg16l1*$^{-/-}$, *Atg16l1*$^{-/-}$*Ifnar*$^{-/-}$ (derived from *Atg16l1;Ifnar*$^{\Delta IEC}$ mice), and *Atg16l1*$^{-/-}$*Ifnlr*$^{-/-}$
774 organoids (derived from *Atg16l1;Ifnlr*$^{\Delta IEC}$ mice) stimulated on day 3 for 48h. **(G)** Viability of
775 organoids from the indicated genotype stimulated 2h post seeding with 20 ng/ml TNF for 24 and
776 48h. For each condition, at least 20 organoids were seeded in 3 different wells (technical
777 triplicate), which was repeated in at least 3 independent experiments with organoids derived
778 from different mice each repeat. Each symbol represents the average of one technical triplicate
779 (or the mean for each stimulation in B) with bars representing mean ± SEM. ns = not significant,
780 *p≤0.05, **p≤0.01, ****p≤0.0001. See also Figure S2.

781

782

783 **Figure 3: TNF and IFNλ synergize to promote RIPK1-dependent cell death in small**
784 **intestinal organoids. (A)** Representative images of Hoechst (blue) and PI (red) staining of
785 small intestinal organoids from WT (*Atg16l1*$^{+/+}$) and *Atg16l1*$^{\Delta IEC}$ mice (*Atg16l1*$^{-/-}$) cultivated in
786 ENR medium for 3 days and stimulated with ± 20 ng/ml TNF, ± 1ng/ml IFNλ2 for 48h.
787 Organoids were pre-treated with vehicle control, 100nM Ruxolitinib, 10μM Q-VD-OPh, or 10 μM
788 Nec-1s for at least 30min before TNF+IFNλ2 stimulation. Scale bars represent 1000μm. **(B)**
789 Quantification of organoid viability from (A) at 24 and 48h post-stimulation. For each condition,
790 at least 20 organoids were seeded in 3 different wells (technical triplicate), which was repeated
791 in 3 independent experiments with organoids derived from different mice). **(C-E)** Representative
792 western blot of indicated proteins (C) and quantification of phosphorylated RIPK3 (pRIPK3) (D)
793 and cleaved caspase-3 normalized to β-actin and unstimulated control (E) in lysates from
794 *Atg16l1*$^{+/+}$ and *Atg16l1*$^{-/-}$ organoids stimulated for 2h with 20 ng/ml TNF alone or combined with
795 1ng/ml IFNλ2. C and FL designate cleaved and full length, respectively. **(F-G)** Representative
796 western blot of indicated proteins (F) and quantification of MLKL normalized to β-actin and
797 unstimulated control (G) in lysates from *Atg16l1*$^{+/+}$ organoids stimulated for 24h with 20 ng/ml
798 TNF alone, 1ng/ml IFNλ2 alone or the combination of both. **(H-I)** Viability of organoids derived
799 from WT and *Mlkl*$^{-/-}$ mice treated at day 3 with the indicated combinations of TNF, IFNλ2, and
800 IFNβ for 24h (H) or 48h (I). Each symbol represents the average of one technical triplicate (B, I-
801 J) or protein expression observed from a pool of different wells in an independent experiment
802 (F-H) with bars representing mean ± SEM. ns = not significant, *p≤0.05, **p≤0.01, ****p≤0.0001.
803 See also Figure S2 and S3.

804

805

806 **Figure 4:** ***Virally-triggered intestinal disease in Atg16l1 mutant mice is RIPK3-dependent.***
807 **(A)** Survival over time, cumulative disease score, and weight loss in *Atg16L1*$^{f/f}$, *Atg16L1*$^{\Delta IEC}$,
808 *Atg16L1*$^{f/f}$;*Ripk3*$^{-/-}$, and *Atg16L1*$^{\Delta IEC}$;*Ripk3*$^{-/-}$ mice infected for 10 days with MNV before receiving
809 3% DSS in their drinking water for 6 days. **(B)** Colon length on day 5 post DSS treatment of
810 indicated mice infected with MNV as in (A). **(C)** Representative images of H&E staining (top,
811 scale bar 100μm) and immunofluorescence of ileal crypts from mice in (B) stained for lysozyme
812 (red) and DAPI (blue) (bottom, scale bar 20μm). **(D)** Number of Paneth cells observed in each
813 crypt in mice from each genotype. **(E)** Average proportion of abnormal Paneth cells per crypt
814 observed in each mouse as determined on the basis of whether each Paneth cell displayed a
815 typical staining pattern with distinguishable granules (normal, orange arrow) or depleted and/or
816 diffuse staining (abnormal, white arrow). At least 50 crypts were quantified per mouse. Each
817 symbol represents individual mice with bars representing mean ± SEM from at least two
818 independent experiments (except for Paneth cell abnormality, n=1). ns = not significant,
819 *p≤0.05, **p≤0.01, ***p≤0.001, ****p≤0.0001.

820

821

822 **Figure 5: Intestinal organoids derived from *ATG16L1T300A* homozygous individuals**
823 **exhibit heightened susceptibility to inflammatory factors. (A-B)** Representative images at
824 24h post-stimulation with ± 50 ng/mL hTNFα, ± 100 ng/mL hIFNλ2 (A) and viability over time (B)
825 of human organoids from controls (n = 6 donors homozygous or heterozygous for the non-risk
826 allele) and *ATG16L1*^{T300A} homozygous individuals (n=3 donors). **(C)** Bar graph representation of
827 data from (B) comparing non-risk control and *ATG16L1*^{T300A} homozygous organoids. **(D-E)**
828 Representative pictures at 48h (D) and viability over time (E) of non-risk (n=3) and
829 *ATG16L1T300A* homozygous (n=3) organoids post incubation with pooled serum from healthy
830 donors, patients with a blood stream infection (BSI+ SARS-CoV-2-) or patients with a BSI and
831 infected with SARS-CoV-2 (BSI+ SARS-CoV-2+). **(F)** Bar graph representation of data from (E)
832 comparing non-risk control and *ATG16L1*^{T300A} homozygous organoids. For each condition, at
833 least 20 organoids were seeded in 3 different wells (technical triplicate). Each symbol
834 represents the average viability per donor (calculated from technical triplicates) with bars
835 representing mean ± SEM for each group. For (A-C) 2-5 independent experiments were
836 performed for each organoid donor. For (D-E), one experiment was performed for each
837 organoid donor due to the limited quantity of serum available. ns = not significant, *p≤0.05,
838 **p≤0.01, ****p≤0.0001.

839

Figure 1

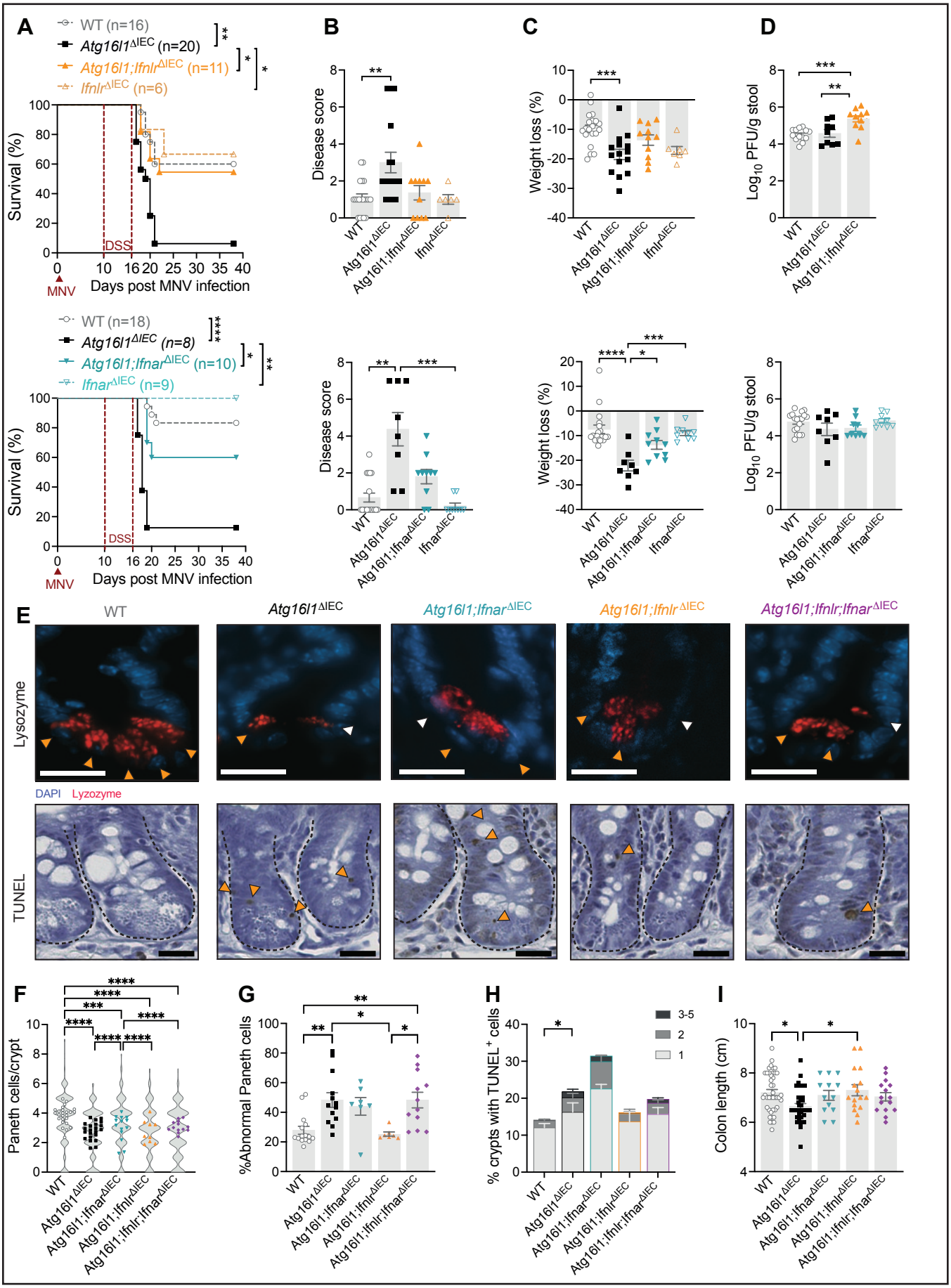
A
WT (n=16)
Atg16l1ΔIEC (n=20)
Atg16l1;IfnlrΔIEC (n=11)
IfnlrΔIEC (n=6)
Survival (%)
DSS
MNV
Days post MNV infection
WT (n=18)
Atg16l1ΔIEC (n=8)
Atg16l1;IfnarΔIEC (n=10)
IfnarΔIEC (n=9)
B
Disease score
C
Weight loss (%)
D
Log10 PFU/g stool
WT
Atg16l1ΔIEC
Atg16l1;IfnlrΔIEC
IfnlrΔIEC
Atg16l1;IfnarΔIEC
IfnarΔIEC
E
WT
Atg16l1ΔIEC
Atg16l1;IfnarΔIEC
Atg16l1;IfnlrΔIEC
Atg16l1;Ifnlr;IfnarΔIEC
Lysozyme
DAPI Lyzozyme
TUNEL
F
Paneth cells/crypt
G
%Abnormal Paneth cells
H
% crypts with TUNEL+ cells
3-5
2
1
I
Colon length (cm)

Figure 2

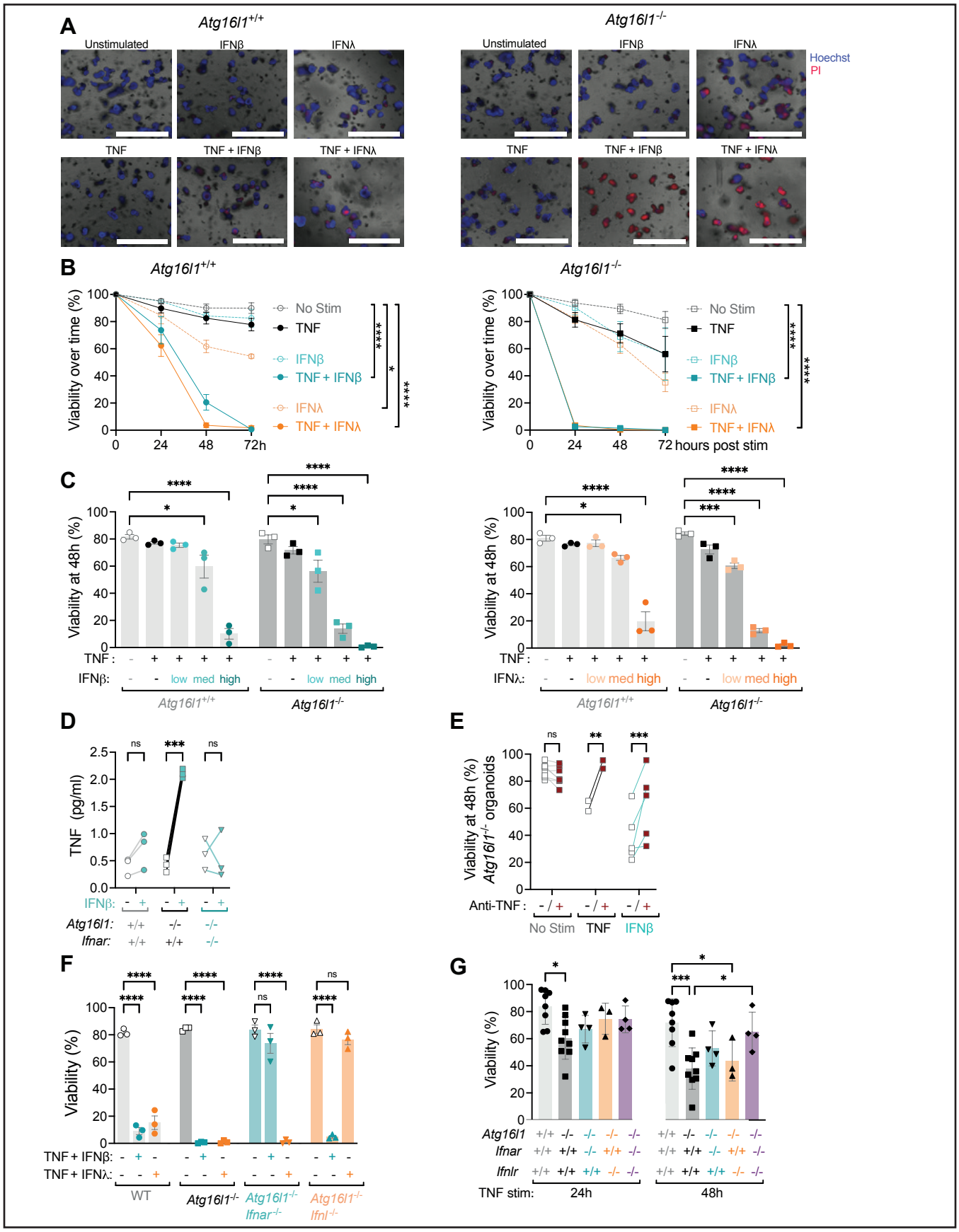
A
Atg16l1+/+
Atg16l1-/-
Unstimulated
IFNβ
IFNλ
TNF
TNF + IFNβ
TNF + IFNλ
Hoechst
PI
B
Viability over time (%)
No Stim
TNF
IFNβ
TNF + IFNβ
IFNλ
TNF + IFNλ
0 24 48 72h
0 24 48 72 hours post stim
C
Viability at 48h (%)
TNF :
IFNβ:
IFNλ:
low med high
D
TNF (pg/ml)
ns
***
IFNβ:
Atg16l1:
Ifnar:
E
Viability at 48h (%) Atg16l1-/- organoids
Anti-TNF :
No Stim
TNF
IFNβ
F
Viability (%)
TNF + IFNβ:
TNF + IFNλ:
WT
Atg16l1-/-
Atg16l1-/- Ifnar-/-
Atg16l1-/- Ifnl-/-
G
Viability (%)
Atg16l1
Ifnar
Ifnlr
TNF stim:
24h
48h

Figure 3

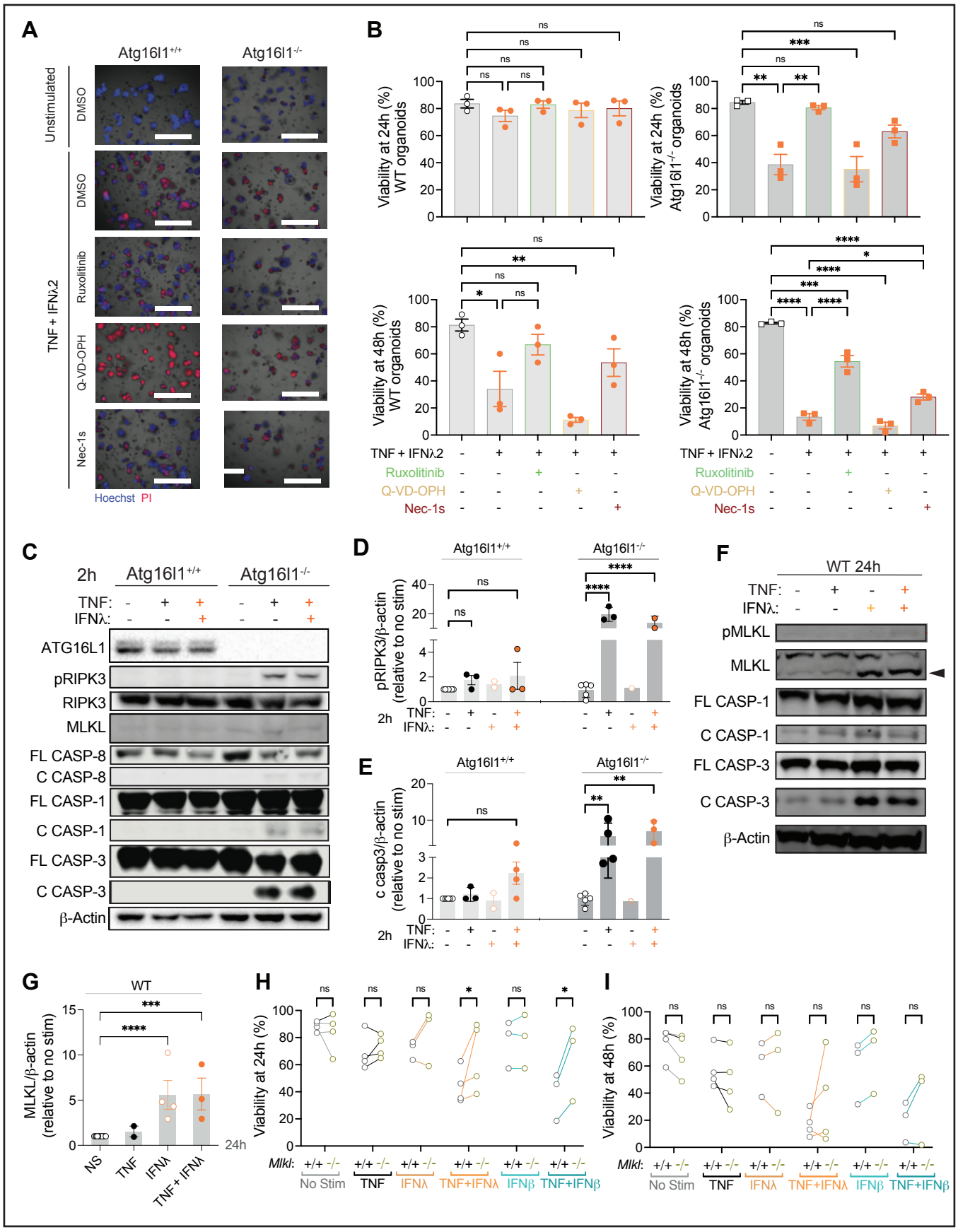
A
Atg16l1+/+
Atg16l1-/-
Unstimulated
DMSO
TNF + IFNλ2
DMSO
Ruxolitinib
Q-VD-OPH
Nec-1s
Hoechst PI
B
Viability at 24h (%) WT organoids
Viability at 24h (%) Atg16l1-/- organoids
Viability at 48h (%) WT organoids
Viability at 48h (%) Atg16l1-/- organoids
TNF + IFNλ2
Ruxolitinib
Q-VD-OPH
Nec-1s
C
2h
Atg16l1+/+
Atg16l1-/-
TNF:
IFNλ:
ATG16L1
pRIPK3
RIPK3
MLKL
FL CASP-8
C CASP-8
FL CASP-1
C CASP-1
FL CASP-3
C CASP-3
β-Actin
D
pRIPK3/β-actin (relative to no stim)
E
c casp3/β-actin (relative to no stim)
F
WT 24h
pMLKL
MLKL
FL CASP-1
C CASP-1
FL CASP-3
C CASP-3
β-Actin
G
WT
MLKL/β-actin (relative to no stim)
NS
TNF
IFNλ
TNF+IFNλ
24h
H
Viability at 24h (%)
Mlkl:
No Stim
TNF
IFNλ
TNF+IFNλ
IFNβ
TNF+IFNβ
I
Viability at 48h (%)

Figure 4

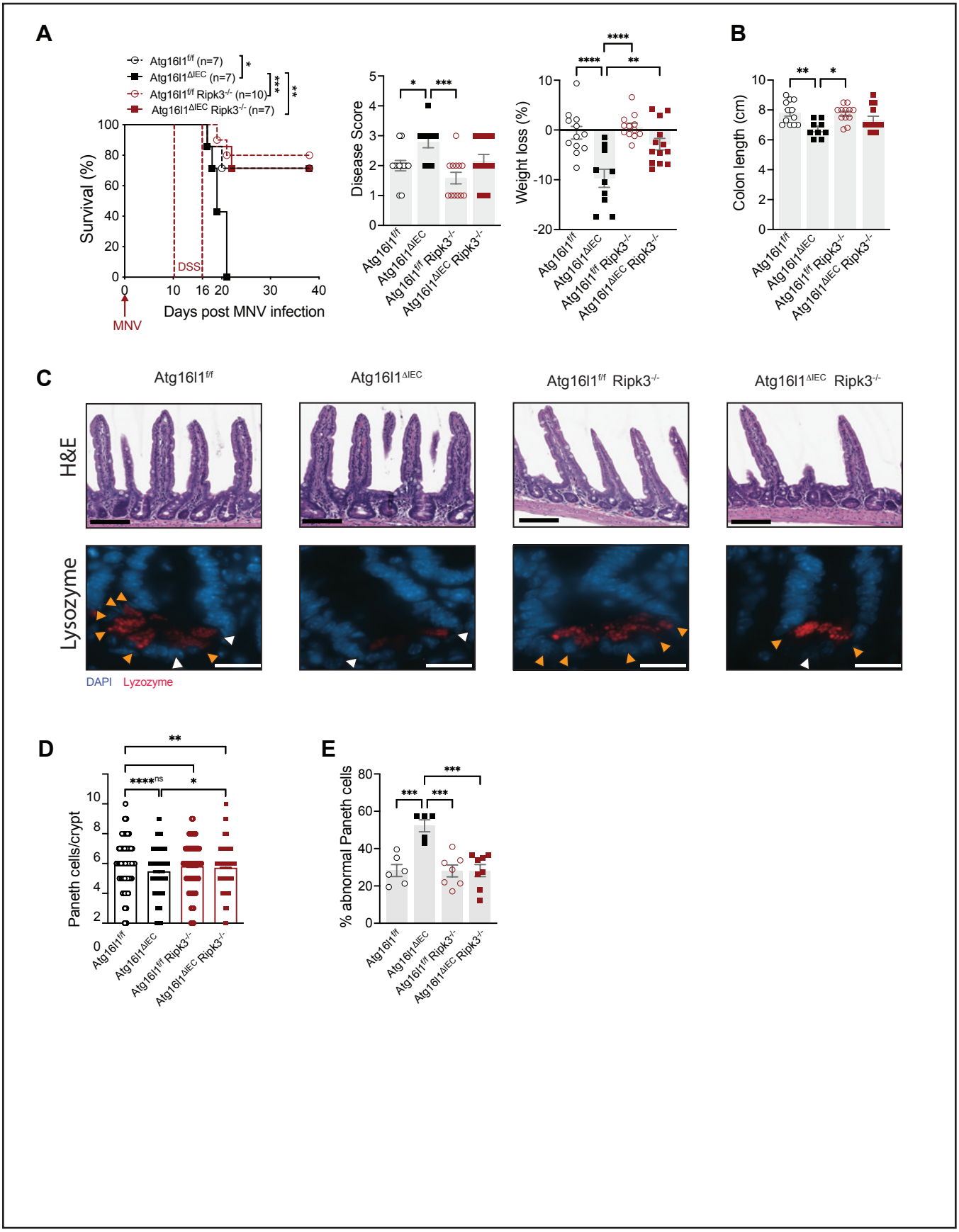
A
Atg16l1f/f (n=7)
Atg16l1ΔIEC (n=7)
Atg16l1f/f Ripk3-/- (n=10)
Atg16l1ΔIEC Ripk3-/- (n=7)
Survival (%)
DSS
MNV
Days post MNV infection
Disease Score
Weight loss (%)
B
Colon length (cm)
C
Atg16l1f/f
Atg16l1ΔIEC
Atg16l1f/f Ripk3-/-
Atg16l1ΔIEC Ripk3-/-
H&E
Lysozyme
DAPI Lyzozyme
D
Paneth cells/crypt
E
% abnormal Paneth cells

Figure 5

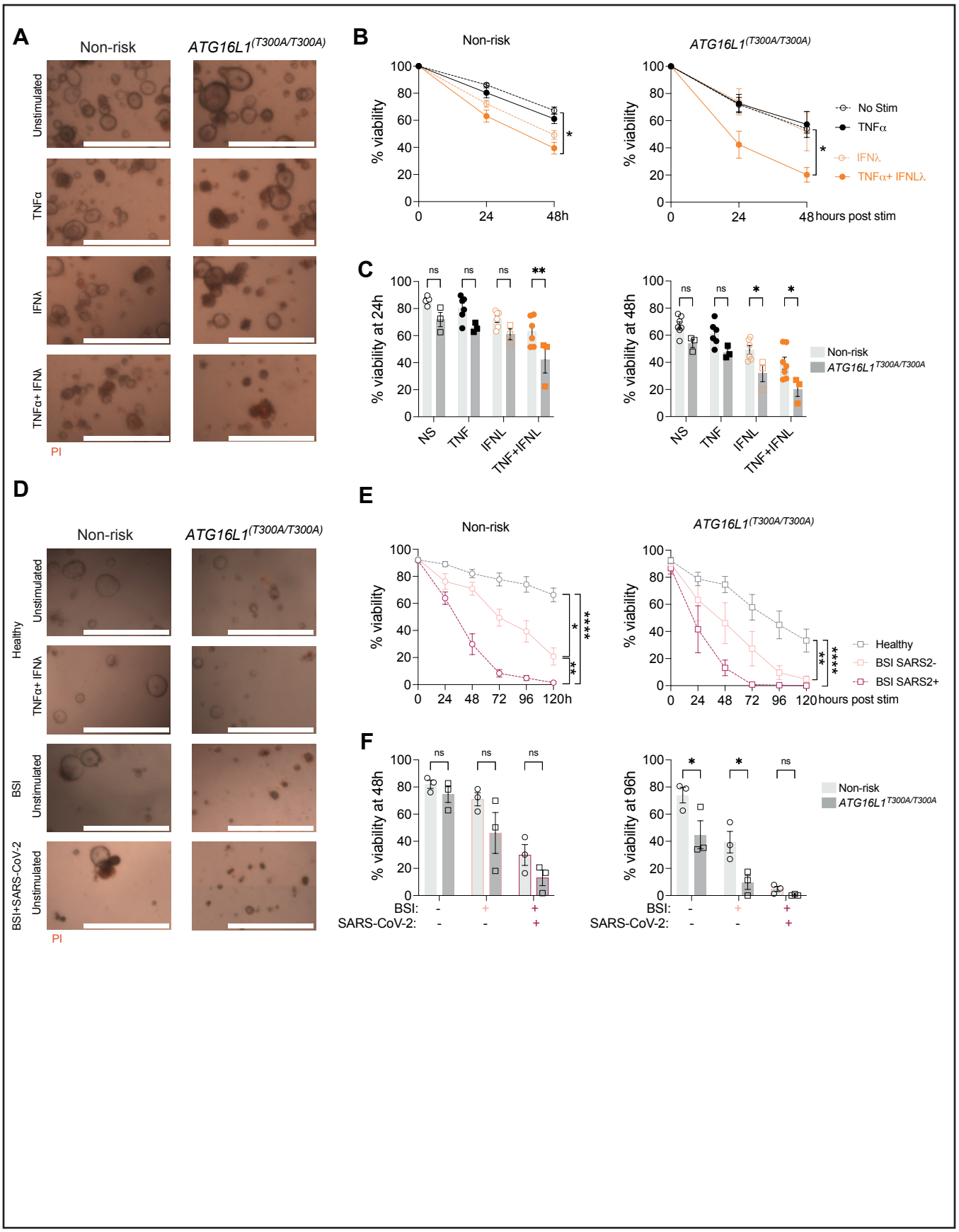
A
Non-risk
ATG16L1(T300A/T300A)
Unstimulated
TNFα
IFNλ
TNFα+ IFNλ
PI
B
Non-risk
ATG16L1(T300A/T300A)
% viability
hours post stim
No Stim
TNFα
IFNλ
TNFα+ IFNLλ
C
% viability at 24h
% viability at 48h
NS
TNF
IFNL
TNF+IFNL
Non-risk
ATG16L1T300A/T300A
D
Healthy
BSI
BSI+SARS-CoV-2
E
Healthy
BSI SARS2-
BSI SARS2+
F
% viability at 96h
BSI:
SARS-CoV-2: